

Electroreduction of CO₂ by Ni sites on nitrogen-doped carbon aerogels from glucose

Leyu Yang¹, Zhiyan Sun², Li Huang¹, Xin Wang¹ ✉, Chunhui Li¹

¹School of Chemistry, Zhengzhou University, Zhengzhou 450001, People's Republic of China

²Department of Disease Prevention and Control, The 988th Central Hospital of PLA, Zhengzhou 450001, People's Republic of China

✉ E-mail: wangxin0620@zzu.edu.cn

Published in Micro & Nano Letters; Received on 15th October 2019; Revised on 14th January 2020; Accepted on 13th February 2020

Electrocatalytic CO₂ reduction has offered a promising route for managing the global carbon balance, but presents challenges because of the lack of highly efficient and low-cost electrocatalyst. Compared with the dispersity of metal active sites, the porous structure of the substrate is more significant for the catalytic performance and the design and fabrication of substrate are often the key points and difficulties for electrocatalysts. Herein a facile method to disperse Ni active sites on nitrogen-doped carbon aerogels with high surface area and porosity is reported. Firstly, hydrophilic polysaccharides were prepared by the hydrothermal process of glucose, followed by ultrasonic mixing with Ni complex and melamine. Secondly, calcination was used to increase the surface area and conductivity of the freeze-dried mixture. The Ni/N-C catalyst exhibited good activity with a Faradaic efficiency for CO production of about 95% and a current density of ~8 mA cm⁻² at an overpotential of 750 mV. The result presents helpful guidelines for the rational design and accurate modulation of low-cost and efficient catalysts.

1. Introduction: Converting CO₂ into chemical fuels using electricity under relative mild condition is one of the hot topics for chemical and materials scientists due to the environmental protection and market economies issues [1–4]. The design of robust and low-cost catalysts to convert greenhouse CO₂ into valuable chemicals is an urgent need. Ideal catalysts should have a low overpotential to drive CO₂ reduction and a large turnover frequency (TOF) and be highly selectivity and durable. Structurally, highly dispersed metal sites on the substrate and abundant nanopores and mesopores for species transfer are both important for electrocatalysts [5–9]. Thus, the construction of porous substrate with anchored sites to stabilise the metal species has been the central question for fabrication highly efficient electrocatalysts. According to kinds of literature reported, single-Ni-atom catalysts favour the CO₂ reduction while Ni nanoparticles favour the hydrogen evolution reaction (HER). Therefore, proper Ni source and porous matrix should be chosen properly to prevent the migration of metal and enhance the atom economy.

Recently, significant research efforts have been focused on fabricating pore structure as a supporter to suppress the metal nanoparticles formation and facilitate the mass transportation of reactants and products [2, 5]. For instance, sacrificial templates such as SiO₂ and ZnO have been used to form active sites on the surface followed by the dissolution in basic solution [10–13], unexpectedly manipulation of sacrificial template method are often inconvenient and wasteful. Metal-organic frameworks (MOFs) have also been adopted to induce metal atoms within their cavities. However, the ligands of these MOFs are not cheap and formation of MOFs are only effective for extremely limited metals and ligands, such as only Co and Zn can react with methylimidazole to form ZIF-67 and ZIF-8 [14–18], other transition metal Fe, Ni and Cu cannot lead to analogous porosity for the coordination ability difference of these first-row transition metal ions. To tackle this challenge, facile and low-cost synthetic strategies should be explored to realise the dispersion of Ni sing-atom on porous carbon supporter as electrocatalyst for CO₂ reduction reaction (CO₂ RR).

Here, we have dispersed mononuclear Ni complex on polysaccharide followed by calcination to Ni/N-doped carbon aerogels (Ni/N-C) as CO₂ electrocatalysts with relatively selectivity and efficiency. Briefly, hydrophilic polysaccharides were firstly

prepared via hydrothermal reaction of a glucose solution containing sodium borate. The as-obtained brown product was ultrasonic dispersed with mononuclear Ni complex and melamine to get an even aqueous solution followed by freeze-drying. Finally, calcination of the polysaccharide at Ar atmosphere realised nitrogen doping of carbon aerogels by pyrolysis product of melamine. Meanwhile, carbonisation of polysaccharide and Ni complex were accomplished and endowed with benign electrical conductivity, which is significant for electrocatalysts.

2. Experimental section

2.1. Materials and physical measurements: All the reagents were of analytical grade and were acquired from Sinopharm Chemical Reagent Company, China. The crystal structure and phase purity were characterised by using an X'Pert PRO X-ray diffractometer (XRD) with Cu K α radiation ($\lambda = 1.5406 \text{ \AA}$) in the 2θ range of 5°–80°. Transmission electron microscopy (TEM) was performed using an FEI Tecnai G2 F20 S-Twin microscope working at an acceleration voltage of 200 kV. X-ray photoelectron spectroscopy (XPS) was performed using Kratos Axis Ultra DLD X-ray Photoelectron Spectrometer. All the peaks were calibrated with C 1 s spectrum at a binding energy of 284.8 eV.

2.2. Synthesis of polysaccharide: The preparation of polysaccharide is based on the way reported in previous studies [19]. Generally, 250 mg of sodium borate and 6.5 g of glucose were dissolved in 15 ml distilled water and then placed in a Teflon-lined autoclave and sealed. The mixture was then heated to 180°C for 8 h under self-generated pressure. Deep brown and mechanically stable monoliths are obtained, washed with massive water and ethanol to remove non-incorporated soluble compounds. Then the product was freeze-dried for further use and the colour turned to light brown.

2.3. Synthesis of the Ni/N-C: 100 mg of polysaccharide, 100 mg of melamine, 1 mg of Ni(OAc)₂·4H₂O, 2 mg of 1,10-phenanthroline monohydrate were ultrasonic dispersed in 20 ml of water for 15 min followed by freeze-drying. The as-obtained product was ground to powders and then placed in a porcelain boat. Then, the boat was annealed at 750°C under Ar for 2 h with the heating rate of 5°C/min. The colour the powders changed from brown to

black indicating the formation of carbon and disappearance of polysaccharide polymer. After cooling down to room temperature, the product was leached at 80°C in 0.5 M H₂SO₄ for 12 h to remove metal particles and unstable species.

2.4. CO₂ RR measurements by glassy carbon electrode (GCE): All electrochemical measurements were carried out at ambient temperature. To prepare the catalyst ink, 5 mg of catalyst and 25 µl of 5% Nafion 117 solution, as a conducting binder, were introduced into 975 µl of water–isopropanol solution with equal volumes of water and isopropanol and sonicated for 3 h. The ink was then drop cast onto the GCE with a disk diameter of 5 mm (Pine instrument) and naturally dried. The working electrode modified with catalyst and the reference electrode (saturated Ag/AgCl electrode) were placed in the cathodic compartment. The counter electrode (graphite rod) was placed in the anodic compartment. Each compartment contained ~30 ml electrolyte (0.5 M KHCO₃), leaving a headspace of ~25 ml. The electrolyte was pre-saturated with N₂ (pH = 8.4) or CO₂ (pH = 7.4). For CO₂ RR electrocatalysis, a flow of 20 sccm of CO₂ or N₂ was continuously bubbled into the electrolyte to maintain its saturation. Cyclic voltammetry (CV) and polarisation curves were carried out at a scan rate of 50 and 10 mV/s, respectively. All the potential readings were iR-corrected unless otherwise specified.

2.5. CO₂ RR measurements by gas diffusion electrode (GDE): Platinum gauze electrode was used as counter electrode and two compartments separated by a piece of Nafion-115 proton exchange membrane as the separator. The CO₂ RR measurements using GDE and H cell were the same as the above procedure.

2.6. Product analysis: In order to analyse the products and their Faradaic efficiency, electrolysis was conducted at a few selected potentials for 1–5 h. During the electrolysis, gaseous products in the headspace of the cathodic compartment were periodically vented into a gas chromatograph (GC, Agilent 7890B) equipped with a molecular sieve 5 Å and two porapak Q columns. Argon was used as the carrier gas. The concentration of H₂ was analysed by a thermal conductivity detector (TCD), and the concentration of CO was analysed by a flame ionisation detector (FID) with a methaniser. The concentration of gaseous products was quantified by the integral area ratio of the reduction production to standards. Their Faradaic efficiency was calculated as below:

$$\text{FE}(\%) = \frac{Q_{\text{CO}}}{Q_{\text{tot}}} \times 100\% = \frac{\left(\frac{v}{60 \text{ s/min}}\right) \times \left(\frac{x}{24,000 \text{ cm}^3/\text{mol}}\right)}{j} \times 100\%$$

where $v = 20$ sccm is the flow rate of CO₂, x is the measured concentration of product in 1 ml sample loop based on the calibration of the GC with a standard gas, $N = 2$ is the number of electrons required to form a molecular of CO or H₂, F is the Faraday constant (96,500 C mol⁻¹), and j is the recorded current.

3. Results and discussion: Brunauer–Emmett–Teller (BET) measurements of the sample were carried out with nitrogen adsorption at 77 K on a Micromeritics ASAP 2460 instrument. The BET surface area of Ni/N-C was 509.7 m² g⁻¹. Transmission electron microscopy (TEM) image analysis of the Ni catalysts revealed the presence of tiny, nearly spherical nanoparticles of dozens of nanometres, aggregating to create a gel structure with hierarchical porosity. The contrast of the two images shows that the absence of Ni NPs in different regions, as shown in Figs. 1a and b. This is consistent with the XRD patterns (Fig. 1d) which give no peaks of metallic Ni or its compounds. The Ni content in Ni/N-C

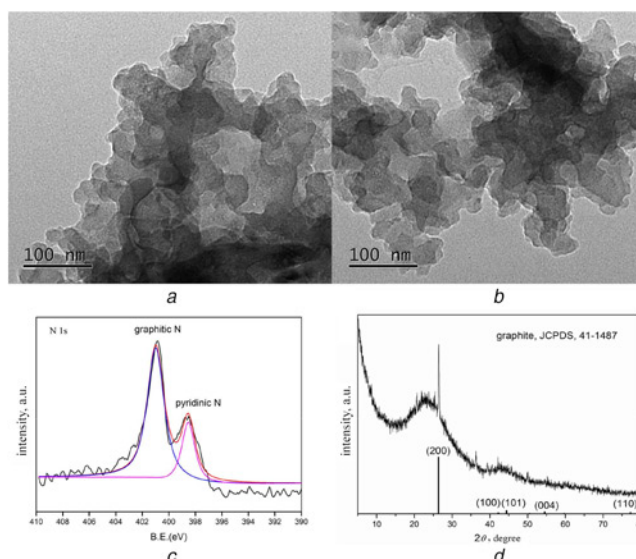


Fig. 1 Morphologies and phase analysis of Ni/N-C
a and b TEM images,
c High-resolution N 1s spectrum,
d XRD patterns of Ni/N-C

was ~0.54 wt% based on inductively coupled plasma optical emission spectroscopy (ICP-OES) measurements. For the Ni catalysts, the high-resolution N 1s XPS spectra can be deconvoluted into two peaks (pyridinic-N, 398.5 eV; graphitic quaternary-N, 400.8 eV) according to their bonding energies (Fig. 1c), showing carbon support was doped by N atoms successfully.

X-ray powder diffraction (XRD) is performed to verify the composition and structure of the Ni catalysts. As exhibited in Fig. 1d, the broad characteristic peak centred at about 24°–26° should be ascribed to the (002) plane reflection of carbon and the sharp peak at 26° corresponds to trace amount of carbon nitride for incomplete pyrolysis of melamine at 750°C for 2 h, which has been widely literature reported [20].

According to previous studies, it has been confirmed that Ni single sites have high CO₂ electroreduction activity. Hence, the electroreduction of CO₂ by the Ni/N-C catalysts is performed in a standard three-electrode cell configuration in 0.5 M KHCO₃ solution purging with excess CO₂ gas.

The activity of Ni/N-C in the electrochemical reduction of CO₂ was evaluated by CV (Fig. 2a) and linear sweep voltammetry (LSV) (Fig. 2b). A cathodic peak at approximately –0.7 V (versus RHE) was observed in both curves while Ni/N-C showed negligible HER activity. In the mass-transport-limited region, at an applied potential of –0.95 V (versus RHE), the GCE decorated by Ni/N-C produced a cathodic current density of 35 mA/cm². Negligible decay was detected after 5 h CV cycles, implying the excellent chemical stability of the Ni atoms in Ni/N-C, which was in consistent with the data shown in Fig. 3a. The Tafel slope (Fig. 2c), which is used to analyse the kinetic feature of the CO₂ reduction reaction on atomic dispersed Ni sites, is 202 mV dec⁻¹ for Ni/N-C, and the data is better than 249 mV dec⁻¹ of Ni SAs/N-C, suggesting a rate-limiting step for CO evolution [21].

As shown in Fig. 4, the GDE electrode decorated by Ni/N-C produced cathodic current density of 30 mA/cm² at the potential of –1.2 V (versus RHE). The inset of Fig. 4 highlights the LSV curves of Ni/N-C at a potential range from 0 to –0.9 V (versus RHE), indicating that the onset potential for CO formation is –0.616 V (versus RHE) while the theoretical potential for CO formation is –0.12 V (RHE). The result has also confirmed the data shown in Fig. 2b. Fig. 3a shows typical current profiles for the catalyst biased at different potentials in CO₂-saturated 0.5 M

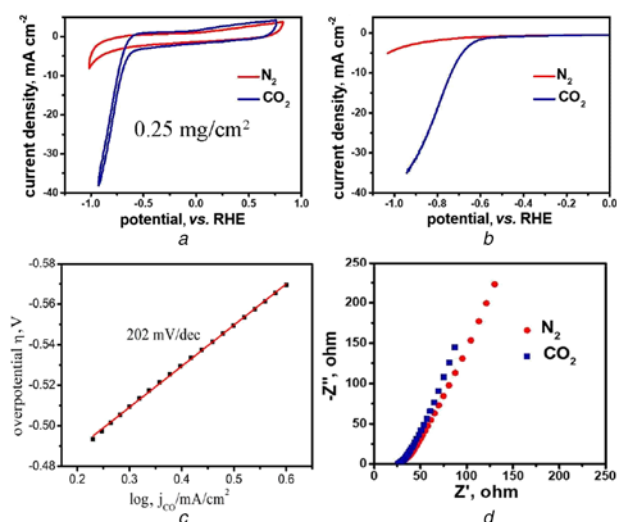


Fig. 2 Electrochemical data of Ni/N-C on GCE
a Cyclic voltammograms of Ni/N-C
b LSV curves acquired in N₂ and CO₂-saturated 0.5 M KHCO₃ solution on GCE
c Tafel slope of Ni/N-C
d Nyquist plots of Ni/N-C on GCE

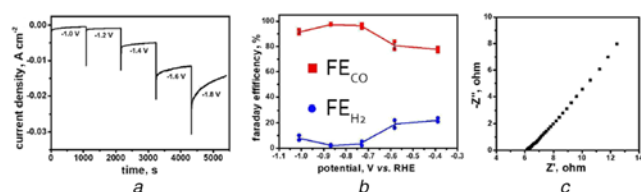


Fig. 3 Electrochemical data of Ni/N-C on GDE
a Typical Chronoamperometric curve of Ni/N-C electrode under bias from -1.0 to -1.8 V versus Ag/AgCl in 0.5 M CO₂-saturated KHCO₃ aqueous solution
b Potential dependence CO and H₂ Faradaic efficiency of Ni/N-C
c Nyquist plots of Ni/N-C on GDE

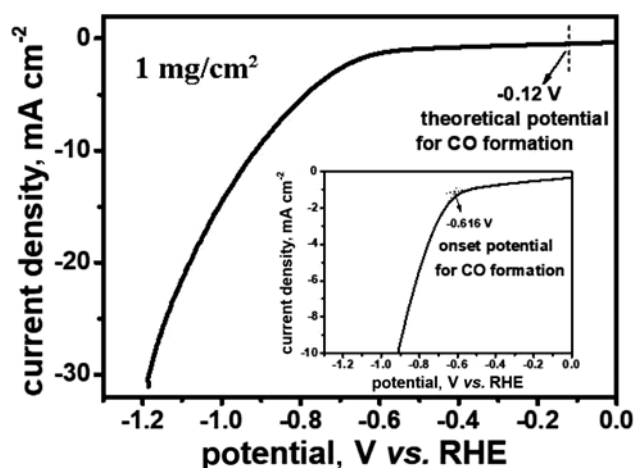


Fig. 4 LSV curve acquired in CO₂-saturated 0.5 M KHCO₃ solution on GDE

KHCO₃ solution for analysis of the reduction products and Faradaic efficiency.

The selectivity and activity of Ni/N-C are confirmed by monitoring of the products formed at different potentials collected over 3 h

Table 1 Comparison of the activities of N,Ni-doped carbon catalysts for CO₂ reduction to CO in 0.5 M KHCO₃

Catalyst	Potential versus RHE, V	Current density, mA/cm ²	Faradic efficiency, %	Reference
Ni/N-C	-0.87	8	95	this work
SE-Ni	-1	18.3	87.80	Yang et al. [2]
SAs@PNC				
Ni SAs/N-C	-1	10.48	70.30	Zhao et al. [21]

of electrolysis with gas chromatographic (GC) analysis, as shown in Fig. 3b.

The Ni/N-C sample can achieve 90% CO and <10% H₂ selectivity at the potential of -0.729 to -1.010 V (all potentials are referenced to RHE), revealing that Ni single atoms are the active sites for the CO₂ electroreduction and CO, compared with H₂, is the dominant product for the all studied potentials. Furthermore, at -0.87 V versus RHE Ni/N-C attained a maximum partial CO current density of ~8 mA cm⁻² with FE of 95%. Considering that Ni SAs/N-C reached 10.48 mA/cm² at -1.0 V and maximum CO FE of 71.9% [21], the catalysts behaviour of the work is relatively close to those of most of the reported catalyst, as shown in Table 1. To gain further insight into CO₂ reduction reaction kinetics, electrochemical impedance spectroscopy (EIS) was carried out and the Nyquist's in Figs. 2d and 3c demonstrate that the charge-transfer process during the CO₂ reduction process, eventually leading to excellent activity and selectivity for CO₂ reduction.

4. Conclusions: In summary, the nitrogen-doped carbon catalyst modified with Ni was synthesised and characterised by BET, XRD, XPS and TEM. The preparation of the substrate based on solvothermal process from glucose was facile and low-cost. Post-synthesis thermal carbonisation is used to increase its surface area and introduce electric conductivity, making it a good candidate for CO₂ electroreduction. Compared with complicated preparation of N-doped carbon supporters, the porous NC support shows favourable mass transfer for CO₂ electroreduction, delivering acceptable activity, selectivity. Our findings shed light on the rational design of low-cost and efficient catalysts for further improving the atom utilisation.

5. Acknowledgments: This work was supported by the National Natural Science Foundation of China (grant no. 21271156).

6 References

- [1] Huan T.N., Ranjbar N., Rousse G., *ET AL.*: 'Electrochemical reduction of CO₂ catalyzed by Fe-N-C materials: a structure-selectivity study', *ACS Catal.*, 2017, **7**, pp. 1520–1525
- [2] Yang J., Qiu Z.Y., Zhao C.M., *ET AL.*: 'In-situ thermal atomization to convert supported nickel nanoparticles into surface-bound nickel single-atom catalysts', *Angew. Chem., Int. Ed.*, 2018, **57**, pp. 14095–14100
- [3] Wang W.Y., Ma M., Kong M.L., *ET AL.*: 'Cobalt carbonate hydroxide hydrate nanowires array: a three-dimensional catalyst electrode for effective water oxidation', *Micro Nano Lett.*, 2017, **12**, (4), pp. 264–266
- [4] Oh S.J., Lee J.H.: 'Preparation and oxidation behavior of cobalt-coated copper powder', *Micro Nano Lett.*, 2017, **12**, (10), pp. 717–721
- [5] Pan Y., Lin R., Chen Y.J., *ET AL.*: 'Design of single-atom Co-N₅ catalytic site: a robust electrocatalyst for CO₂ reduction with nearly 100% CO selectivity and remarkable stability', *J. Am. Chem. Soc.*, 2018, **140**, pp. 4218–4221
- [6] Wang K., Sun Z.Y., Zhu Y., *ET AL.*: 'Effect of different carbon supporter on the Ni/C catalyst for water oxidation', *Micro Nano Lett.*, 2019, **14**, (4), pp. 409–411

- [7] Stevens M.B., Trang C.D.M., Enman L.J., *ET AL.*: 'Reactive Fe-sites in Ni/Fe (oxy)hydroxide are responsible for exceptional oxygen electrocatalysis activity', *J. Am. Chem. Soc.*, 2017, **139**, pp. 11361–11364
- [8] You B., Liu X., Hu G.X., *ET AL.*: 'Universal surface engineering of transition metals for superior electrocatalytic hydrogen evolution in neutral water', *J. Am. Chem. Soc.*, 2017, **139**, pp. 12283–12290
- [9] Zhao Y.F., Jia X.D., Chen G.B., *ET AL.*: 'Ultrafine NiO nanosheet stabilized by TiO₂ from monolayer NiTi-LDH precursors: an active water oxidation electrocatalyst', *J. Am. Chem. Soc.*, 2016, **138**, pp. 6517–6524
- [10] Feng Q.C., Zhao S., Xu Q., *ET AL.*: 'Mesoporous nitrogen-doped carbon-nanosphere-supported isolated single-atom Pd catalyst for highly efficient semihydrogenation of acetylene', *Adv. Mater.*, 2019, **31**, pp. 1901024–1901030
- [11] Han Y.H., Wang Y.G., Chen W.X., *ET AL.*: 'Hollow N-doped carbon spheres with isolated cobalt single atomic sites: superior electrocatalysts for oxygen reduction', *J. Am. Chem. Soc.*, 2017, **139**, pp. 17269–17272
- [12] Meng G., Yang Q., Wu X.C., *ET AL.*: 'Hierarchical mesoporous Nio nanoarrays with ultrahigh capacitance for aqueous hybrid supercapacitor', *Nano Energy*, 2016, **30**, pp. 831–839
- [13] Ma S.S., Su P.P., Huang W.J., *ET AL.*: 'Atomic Ni species anchored N-doped carbon hollow spheres as nanoreactors for efficient electrochemical CO₂ reduction', *Chem. Cat. Chem.*, 2019, **11**, pp. 6092–6098, 10.1002/cctc.201901643
- [14] Wang X.Q., Chen Z., Zhao X.Y., *ET AL.*: 'Regulation of coordination number over single Co sites: triggering the efficient electroreduction of CO₂', *Angew. Chem., Int. Ed.*, 2018, **57**, pp. 1944–1948
- [15] Yin P.Q., Yao T., Wu Y.E., *ET AL.*: 'Single cobalt atoms with precious N-coordination as superior oxygen reduction reaction catalysts', *Angew. Chem., Int. Ed.*, 2016, **55**, pp. 10800–10805
- [16] Wei S.J., Li A., Liu J.C., *ET AL.*: 'Direct observation of noble metal nanoparticles transforming to thermally stable single atoms', *Nat. Nanotechnol.*, 2018, **13**, pp. 856–861
- [17] Lu P.L., Yang Y.J., Yao J.N., *ET AL.*: 'Facile synthesis of single-nickel-atomic dispersed N-doped carbon framework for efficient electrochemical CO₂ reduction', *Appl. Catal., B*, 2019, **241**, pp. 113–119
- [18] Zhang M.L., Wu T.S., Hong S., *ET AL.*: 'Efficient electrochemical reduction of CO₂ by Ni-N catalysts with tunable performance', *ACS Sustain. Chem. Eng.*, 2019, **7**, pp. 15030–15035
- [19] Fellinger T.P., White R.J., Titirici M.M., *ET AL.*: 'Borax-mediated formation of carbon aerogels from glucose', *Adv. Mater.*, 2012, **22**, pp. 3254–3260
- [20] Zhang T., Zhang D., Han X.H., *ET AL.*: 'Preassembly strategy to fabrication porous hollow carbonitride spheres inlaid with single Cu-N₃ sites for selective oxidation of benzene to phenol', *J. Am. Chem. Soc.*, 2018, **140**, pp. 16936–16940
- [21] Zhao C.M., Dai X.Y., Yao T., *ET AL.*: 'Ionic exchange of metal-organic framework to access single nickel sites for efficient electroreduction of CO₂', *J. Am. Chem. Soc.*, 2017, **139**, pp. 8078–8081